Design and Verification of Active Balancing Circuit for Battery Management System Based on a Bidirectional Converter

Chang-Hua Lin, Yu-Lin Lee
National Taiwan University of Science and Technology, Taiwan, R.O.C.

***Abstract*-- This paper presents a modular design and validation for a battery management system (BMS) based on a dual-concentration architecture. The proposed architecture improves the BMS's performance, such as the balancing process and a reduction in the number of components required by the BMS, including power switches, switching arrays, and energy storage elements. Generally, even an active balancing process still causes some energy loss, so this study applies a modified flyback converter with an active clamp for the battery module balancing process, which has a higher conversion efficiency, especially in low-power conditions. The simulation results of the balancing circuit are consistent with the measured results. To quantify the improvement of the balancing strategies on the balancing results, this study also presents four balancing strategies for the proposed BMS, wherein the balancing duration and maximum voltage error of the balancing strategy can be reduced by approximately 34% and 73%, respectively, compared with the worst-case scenario in the four balancing strategies.**

***Index Terms*—active balancing, battery management system, flyback converter, battery modular.**

I. Introduction

Battery power systems are commonly used in many applications, such as energy storage systems, uninterruptible power supplies, and electric vehicles. To achieve the required voltage or capacity level, battery systems should utilize cells connected in series or parallel. However, a cell mismatch problem arises after numerous charge-discharge cycles due to the different chemical and electrical characteristics of the cells. This problem may reduce the available capacity and increase the operational risk of a battery power system. Therefore, the development of a BMS with monitoring, protection, and cell-balancing functions is crucial [1]-[4]. The voltage of the battery power system is increased to reduce the power loss caused by the power transmission. To obtain operational safety in a higher-voltage battery power system, multiple cells must be divided into multiple modules so that the BMS can provide monitoring, cell-balancing, and protection functions to all the cells by modular architecture design. However, this leads to another imbalance problem among the battery modules. To solve the imbalance among the multiple series battery modules, modular architectures were designed.

The main purpose of this study is to integrate cell balancing and module balancing to form a dual-concentration BMS for a high-count series battery system with the following advantages. First, the dual-concentration BMS architecture provides better battery sampling accuracy. Second, the proposed architecture allows scalability of the battery system specification. Finally, the dual-concentration BMS design enables a trade-off between the performance and construction cost of the BMS. In contrast to these new topologies [5]-[6], the proposed topology gives BMS higher operational reliability, sampling accuracy, lower balancing duration, and lower hardware complexity.

Furthermore, the proposed topology can solve the imbalance among battery modules by a modified flyback converter with an active clamp and the imbalance within each module by a bidirectional converter while optimizing the number of circuit components, including switch, inductor, transformer, diode, number of target cells and target modules, transfer range of the cell and module equalization, efficiency of the converter, equalization speed, control simplicity, modularity and cost.

II. Circuit Structure and System Description

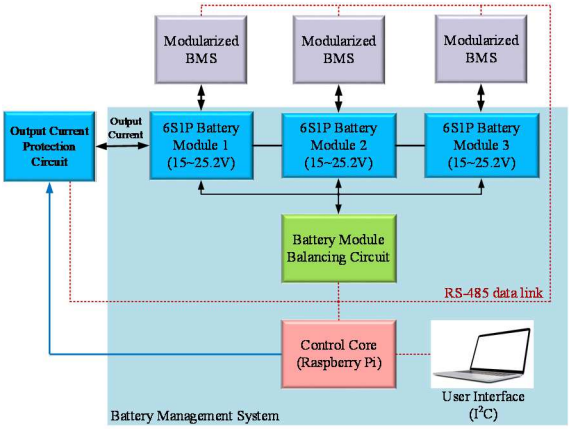

Fig. 1. Block diagram of the proposed BMS.

Fig. 1 shows a block diagram of the proposed BMS, which consists of three 6S1P battery modules with modularized BMSs, a battery module balancing circuit, a control core (Raspberry Pi), a user interface (UI), and an output current protection circuit. The control core can collect all the voltages (differential voltage circuit), currents (hall sensors), and temperatures (k-type thermocouple) from the modularized BMS by using a control core and via an RS-485 data link (Modbus

protocol) so that the proposed BMS provides over-voltage protection (OVP), over-current protection (OCP), over-temperature protection (OTP), under-voltage protection (UVP), under-current protection (UCP), and under-voltage protection (UTP) functions to ensure that the proposed system operates safely. Fig. 2 displays a block diagram of an active cell-balancing system based on a bidirectional converter. This system plays a crucial role in the modular BMS architecture.

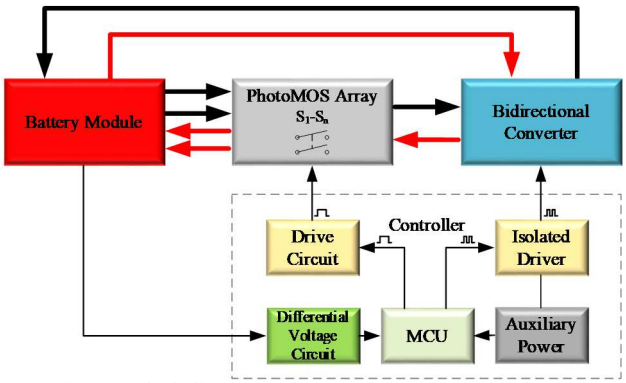

Fig. 2. Block diagram of the modularized BMS based on a bidirectional converter.

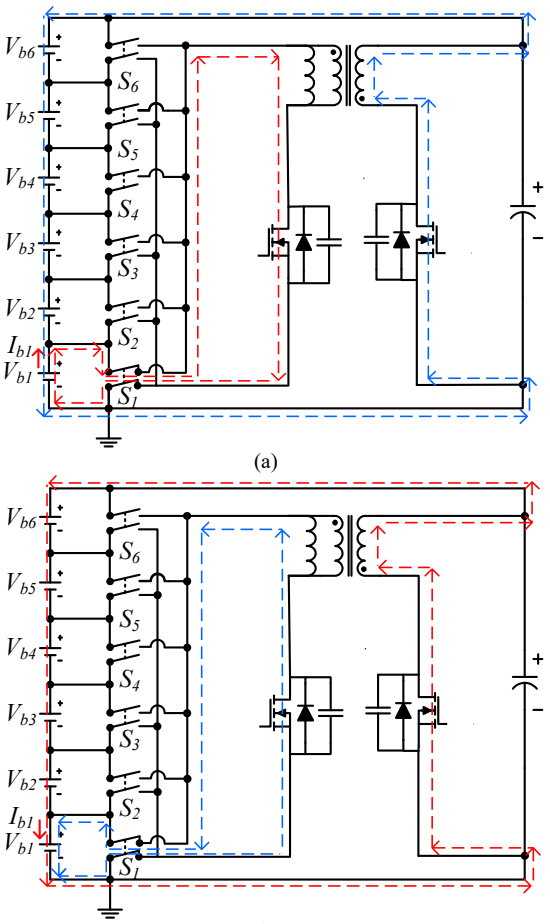

(a)

(b)

Fig. 3. Schematic diagram of an active cell balancing circuit based on a bidirectional flyback converter in (a) boost mode and (b) buck mode.

As shown in Fig. 3, the proposed cell balancing system is realized through the bidirectional flyback converter topology, where S_1-S_n is the photoMOS array. The cell state of charge determines the operation mode of the photoMOS relay and the MOSFETs. For example, when V_{b1} is the highest in the battery module, S_1 is turned on, and bidirectional flyback works as a medium for energy transfer from the first cell to other cells, as shown in Fig. 3(a). In contrast, V_{b1} is less than other cell voltages in the battery module, and the energy is transferred from other cells to the first cell, as shown in Fig. 3 (b). Through a simple architecture with bidirectional energy transfer, modularized BMSs can achieve high balancing efficiency while being inexpensive.

To solve the battery module mismatch problem, this study proposes a battery module balancing circuit. Fig. 4 displays a block diagram of the proposed battery module balancing circuit, which contains a modified flyback converter with an active clamp, a micro controller unit (MCU: dsPIC33FJ64GS606), a metal-oxide-semiconductor field-effect transistor (MOSFET) switching array, an auxiliary power circuit, a differential voltage circuit, and isolated driver circuits. The modified flyback converter with an active clamp is a key part of the proposed circuit.

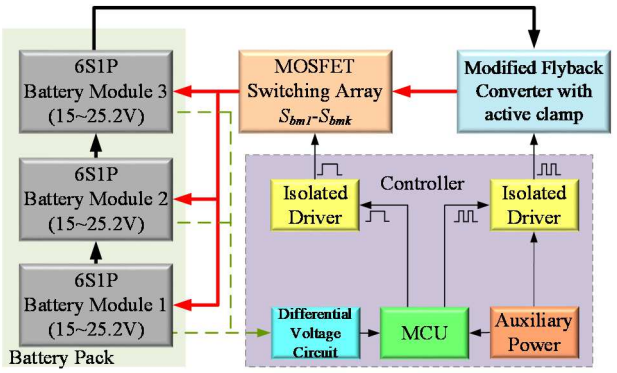

Fig. 4. Schematic diagram of an active cell balancing circuit based on a bidirectional flyback converter in (a) boost mode and (b) buck mode.

The balancing strategy of the proposed battery module balancing circuit is depicted in Fig. 5, where V_{er} is the preset minimum voltage error for activating the balancing process. The module balancing function drives the battery module balancing circuit to provide the preset balancing current (constant current mode). This flowchart explains how the battery module balancing circuit works. Through the control flow, the battery module balancing circuit can converge the voltage of the battery modules. First, the MCU collects the voltages of the battery modules through a differential voltage circuit. Second, the proposed system determines whether the battery module balancing circuit should begin executing the balancing function, depending on the calculated ΔV_{bmn} value for each battery module. Third, the circuit extracts energy from the battery pack and gives it to the battery module with the lowest voltage. The balancing process is maintained until the timer reaches T_1, which can be determined by the user and should not be excessively long to avoid a temperature rise. Finally, the MCU deactivates the module balancing function and waits for the next balance decision.

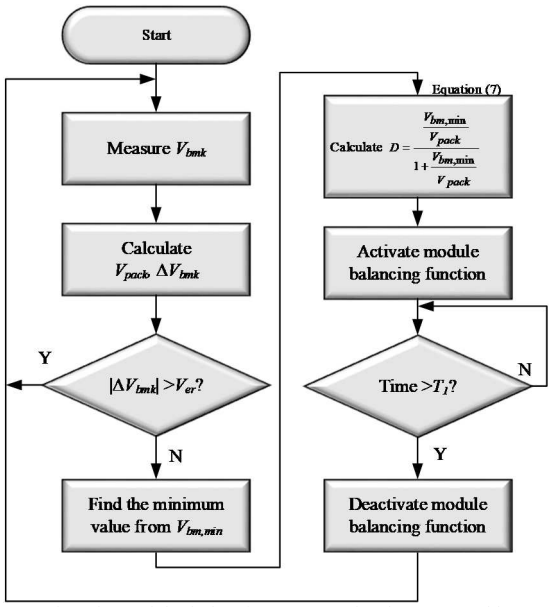

Fig. 5. Flowchart of the balancing strategy for the proposed battery module balancing circuit.

The proposed battery module balancing circuit contains a modified flyback converter with an active clamp, as displayed in Fig. 6, where N is the turn ratio of the transformer; I_1 is the current extracted from the battery pack; I_2 is the battery module balancing current; L_m is the magnetizing inductance of the transformer; S_{bmk} is the MOSFET array; Q_1 is the MOSFET used for power switching; and Q_2 and C_r are the key parts of the converter's active clamp function.

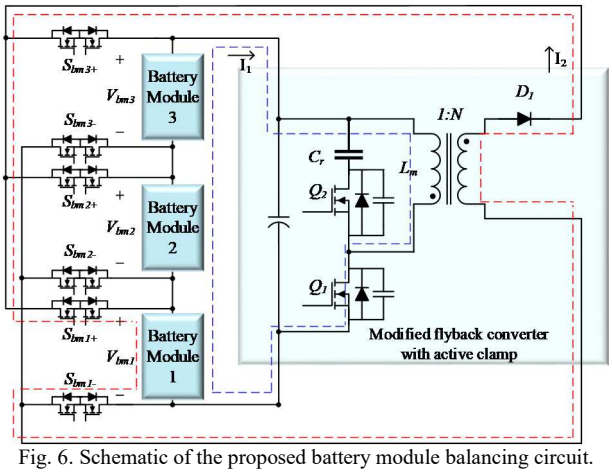

Fig. 6. Schematic of the proposed battery module balancing circuit.

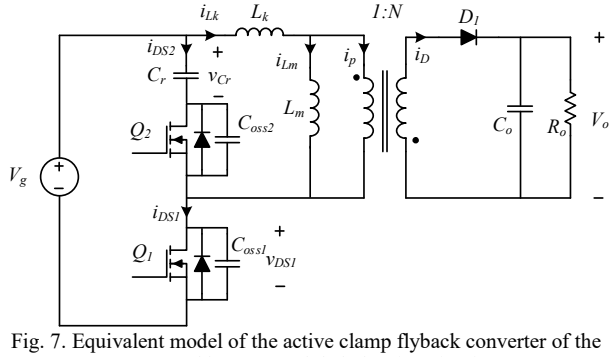

Fig. 7. Equivalent model of the active clamp flyback converter of the proposed battery module balancing circuit.

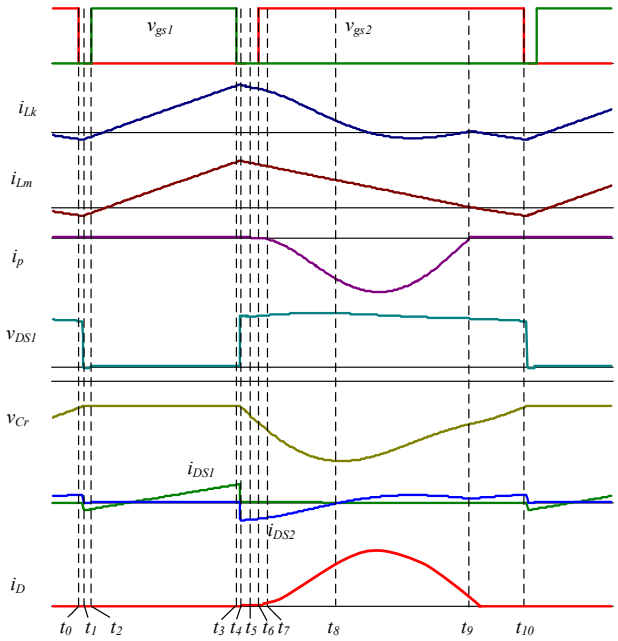

Fig. 8. Key waveforms of the proposed module balancing circuit.

The modified flyback converter with an active clamp used in this study recycles the energy stored in the leakage inductance of the transformer and the parasitic capacitance of the MOSFET to minimize the spike voltage at the primary side of the transformer and improve the converter efficiency. Fig. 7 shows the equivalent model of the modified flyback converter with an active clamp used in the proposed battery module balancing circuit.

III. Design Considerations

The key parameters of the active clamp flyback converter used in the proposed battery module balancing circuit are listed in Table 1. The adopted lithium-ion battery module has a 6S1P configuration with a rated capacity of 2600 mAh and a voltage range of 15–25.2 V. Moreover, the lithium-ion battery pack consists of three battery modules. The battery module balancing current is preset at 1 A according to the cell's rated capacity and the PCB trace width.

TABLE 1
PARAMETERS OF THE ADOPTED MODIFIED FLYBACK CONVERTER WITH ACTIVE CLAMP

Parameter	Value
Output power P_o	15 W ~ 50 W
Input voltage V_G	45 V ~ 75 V (18S1P)
Output voltage V_o	15 V ~ 25.2 V (6S1P)
Battery module balancing current I_2	0 ~ 2 A
Duty cycle D	23% ~ 47.5%
Operation frequency F_s	100 kHz

1) *Determination of the transformer turn ratio*

To obtain higher active balancing performance, in this study, an active clamp flyback converter was employed and designed in DCM. The relationship between V_o and V_g can be obtained by using (1) and (2), *Gain* is the voltage gain of the converter, and D is the duty cycle.

$$\int_0^{Ts} L_m i_{Lm}(t)\,dt = \int_{t_1}^{t_3} V_g\,dt + \int_{t_7}^{t_9}\left(-\frac{V_o}{N}\right)dt = 0 \quad (1)$$

$$Gain = \frac{V_o}{V_g} = N\frac{D}{1-D} \quad (2)$$

If the circuit functions are in the worst condition—when V_g has its lowest value of 45 V and V_o has its highest value of 25.2 V—the system achieves the maximum duty cycle of 47.5%. Therefore, the turn ratio can be obtained as follows:

$$N = \frac{V_{o,max}(1-D)}{V_{g,min}D} = \frac{25.2\,V\times(1-0.475)}{45\,V\times0.475} = 0.61 \quad (3)$$

The practical design, the turn ratio N is selected as 0.667 to avoid the worst-case scenario and implement the system conveniently.

2) *Determination of the magnetizing inductance L_m*

The adopted modified flyback converter with an active clamp achieves the ZVS operation of Q_1 through the current reversal of L_m by clamp capacitor C_r. To ensure the full-range ZVS operation of Q_1, L_m should be determined using (4) and (5), where $\triangle I_{Lm}$ is the current ripple of L_m.

$$\triangle I_{Lm} \le 2I_2\left(1+\frac{V_{o,max}}{NV_{g,min}}\right) = 2\cdot 1\,A\cdot\left(1+\frac{25.2\,V}{\frac{1}{3}\cdot 45\,V}\right) \approx 5.36\,A \quad (4)$$

$$L_m \le \frac{V_{g,min}D_{max}}{\triangle I_{Lm}f_s} = \frac{45\,V\cdot0.475}{5.36\,A\cdot10^5\,Hz} \approx 40\,\mu H \quad (5)$$

In the practical design, L_m is approximately 39 μH.

3) *Selection of the clamp capacitance C_r*

To further increase the converter's efficiency, the proposed system ensures ZCS operation of D_1. C_r and L_k resonate from t_6 to t_9. At $t = t_9$, the current becomes 0, and D_1 performs the ZCS operation to reduce the loss caused during its switched-off period. Therefore, C_r can be obtained using (11), where L_k is measured using an LCR meter.

$$C_r \le \frac{\left(\frac{(1-D_{max})}{\pi f_s}\right)^2}{L_k} = \frac{\left(\frac{(1-0.475)}{\pi\cdot10^5}\right)^2}{2.1\mu H} = 1.33\,\mu F \quad (6)$$

In the practical design, the clamp capacitance C_r is 470 nF.

IV. Implementation and Verification

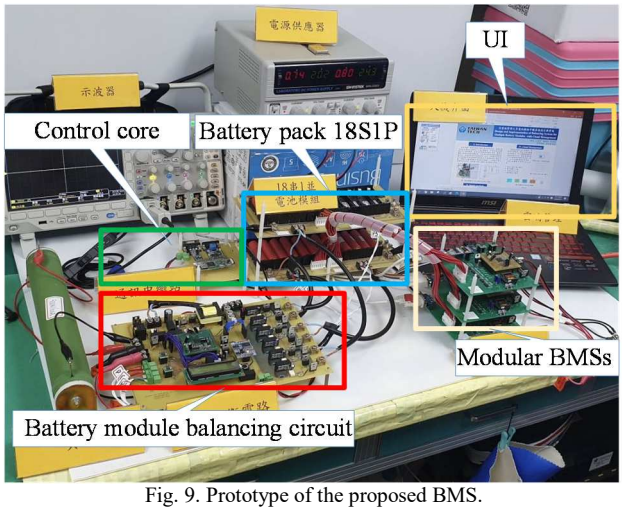

Fig. 9. Prototype of the proposed BMS.

Experiments were conducted to confirm the high performance of the proposed BMS with the fourth balancing strategy. A prototype of the proposed BMS was developed and implemented. This prototype contained modularized BMSs, a battery module balancing circuit, a control core and a UI, as displayed in Fig. 9. The cells used in the BMS were lithium ternary cells (UR18650NSX, Panasonic) with a capacity of 2600 mAh and a voltage range of 2.5–4.2 V. The battery pack contained 18 lithium ternary cells in series; therefore, the battery pack voltage Vpack was 45–75.6 V. A single battery module was composed of six cells in series and had a voltage range of 15–25.2 V. The balancing current I2 was 1 A, and the modularized BMS balancing current was also preset to 1 A.

A simulation and an experiment were conducted in the worst case to confirm the ZVS and ZCS operation of the modified flyback converter with an active clamp under the battery module's specification. As displayed in Fig. 10, the gate-source voltages across Q_1 and Q_2 were v_{gs1} and v_{DS2}, respectively, and the drain-source voltages across Q_1 and Q_2 were v_{DS1} and v_{DS2}, respectively. The leakage inductance current flowing through the inductor was i_{Lk}. The voltage and current of D_1 were v_D and i_D, respectively. The experimental results are shown in Fig. 11. Fig. 10 and 11 indicate that Q_1 and Q_2 could achieve ZVS. Moreover, D_1 could achieve ZCS in both simulation and experiment.

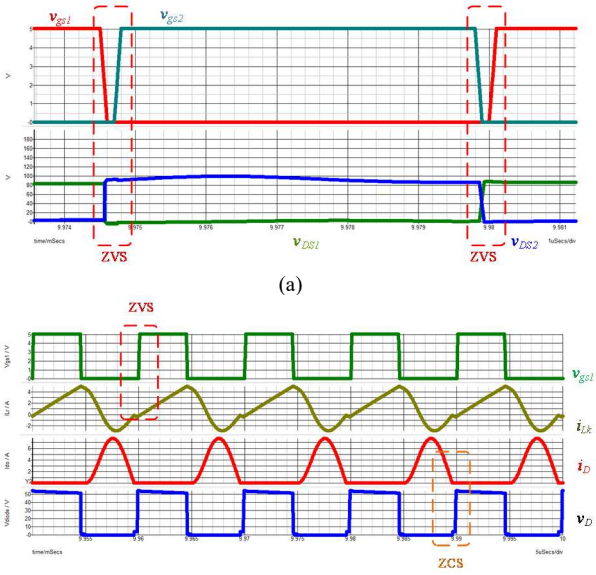

Fig. 10. Simulated waveforms of the developed prototype: (a) ZVS operation and (b) ZCS operation.

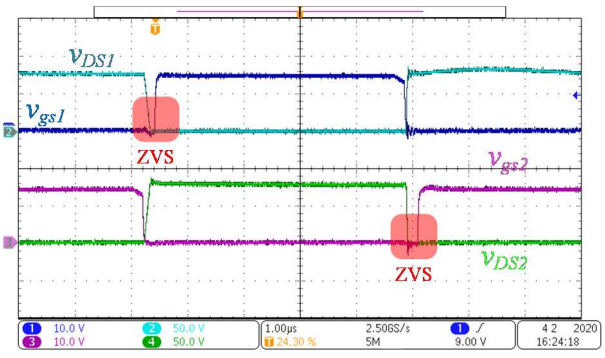

(a)

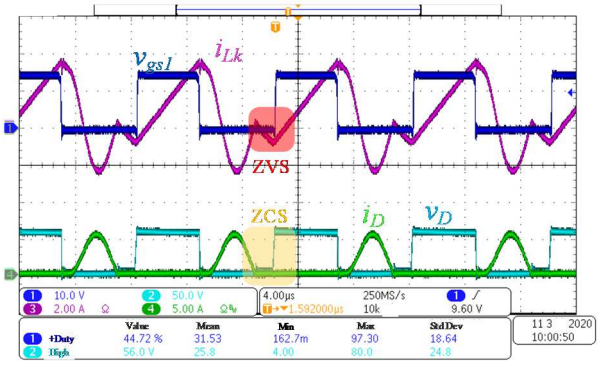

(b)

Fig. 11. Measured waveforms of the developed prototype: (a) ZVS operation and (b) ZCS operation.

This study aimed to set the nearly widest range of the voltage differences (from 2.7 V to 4.0 V) than those of other research to prove the feasibility and performance of the proposed architecture. The BMS operated under the following conditions: the balancing current was preset at 1 A in the modularized BMSs and battery module balancing circuit, and the balancing process had a duration of 30 s (T1). All the experimental results of the battery voltage variation over time when using the four balancing strategies are illustrated in Fig. 12.

From Fig. 12, the final balancing duration and maximum voltage error were determined. As shown in Fig. 12(a), when the first method was used, the balancing process lasted 12602 s (3282 + 9320 s), and the voltage error was 80 mV. In Fig. 12(b), when the second method was used, the balancing process lasted 14752 s (8863 + 5889 s), and the voltage error was 110 mV. When using the third method, as shown in Fig. 12(c), the balancing process lasted 9142 s, and the voltage error was 70 mV. Finally, when using the fourth method, as shown in Fig. 12(d), the balancing process lasted 9767 s (9142 + 625 s), and the voltage error was 30 mV.

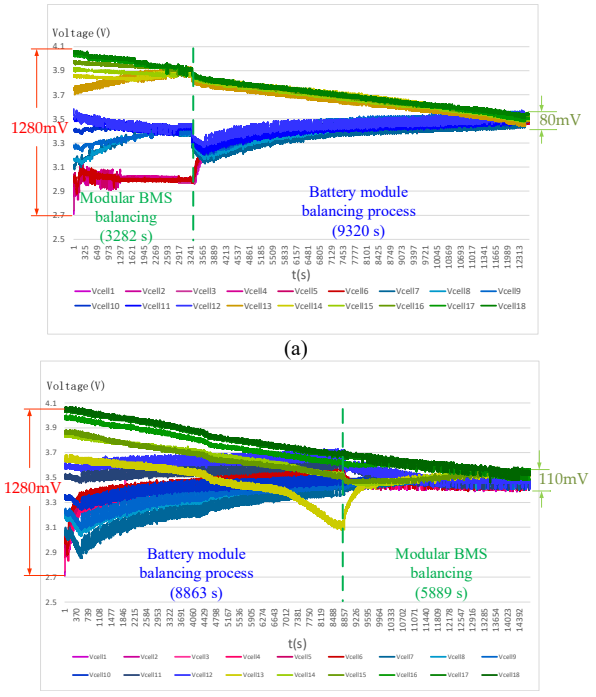

Fig. 12 Measured voltage of each cell under different balancing strategies: (a) the first method, (b) the second method, (c) the third method, and (d) the fourth method.

V. Conclusions

In this study, a modular design for an 18S1P BMS based on a dual-concentration architecture was developed and evaluated, showing the possibility that the proposed BMS can extend the battery system specifications to achieve monitoring, balancing, and protection functions. Moreover, a modified flyback converter with an active clamp, regarded as the battery module balancing circuit, was analysed and found to achieve both ZVS and ZCS for increasing conversion efficiency. In addition, the proposed BMS can use different balancing strategies in different situations. When the proposed BMS operates under the test condition using the fourth method (considering both the voltage error and balancing duration), the balancing duration was 9767 s, and the maximum voltage error was less than 30 mV (33.80% and 72.73% lower than the corresponding values obtained with the second method, respectively). Finally, the proposed dual-concentration BMS underwent a comprehensive comparison with the existing technologies in various aspects of system characteristics to show its outstanding advantage.

Acknowledgment

This research was funded by the National Science and Technology Council, Taiwan, R.O.C., grant number MOST 111-2221-E-011-071, MOST 111-3116-F-011-005, and MOST 111-2622-8-005-003-TE1.

References

[1] J Guo, F.M. Jiang, A novel electric vehicle thermal management system based on cooling and heating of

batteries by refrigerant, Energy Conversion and Management 226 (2020) 113473.
[2] S. Li, C. Gu, P. Zhao, S. Cheng, Adaptive energy management for hybrid power system considering fuel economy and battery longevity, Energy Conversion and Management 235 (2021) 114004.
[3] Y. Zhou, S. Cao, Coordinated multi-criteria framework for cycling aging-based battery storage management strategies for positive building–vehicle system with renewable depreciation: Life-cycle based techno-economic feasibility study, Energy Conversion and Management 226 (2020) 113473.
[4] Y.F. Wang, J.T. Wu, Thermal performance predictions for an HFE-7000 direct flow boiling cooled battery thermal management system for electric vehicles, Energy Conversion and Management 207 (2020) 112569.
[5] A. Manenti, A. Abba, A. Merati, S.M. Savaresi, A. Geraci, A New BMS Architecture Based on Cell Redundancy, IEEE Trans Ind Electron 58 (2011) 4314–4322.
[6] M.Y. Kim, C.H. Kim, J.H. Kim, G.W. Moon, A Chain Structure of Switched Capacitor for Improved Cell Balancing Speed of Lithium-Ion Batteries, IEEE Trans Ind Electron 61 (2014) 3989–3999.